ConBRepro
X CONGRESSO BRASILEIRO DE ENGENHARIA DE PRODUÇÃO
EVENTO ON-LINE
02 a 04 de dezembro 2020

Application of MobileNet Convolutional Neural Network for Classification of Pediatric Images of Chest X-rays

Gabrielly Balsarin Pinto
Advanced Campus in Jandaia do Sul, Federal University of Parana, Jandaia do Sul, Brazil
Henrique Kiyoshi Oshiro
Advanced Campus in Jandaia do Sul, Federal University of Parana, Jandaia do Sul, Brazil
Helena Macedo Reis
Advanced Campus in Jandaia do Sul, Federal University of Parana, Jandaia do Sul, Brazil
Rafael Germano Dal Molin Filho
Advanced Campus in Jandaia do Sul, Federal University of Parana, Jandaia do Sul, Brazil
Rodrigo Clemente Thom de Souza
Advanced Campus in Jandaia do Sul, Federal University of Parana, Jandaia do Sul, Brazil
Production Engineering Graduation Program, State University of Maringa, Maringa, Brazil

Abstract: Lung diseases are a serious problem in the lives of many people and their correct diagnosis is absolutely important. For this reason, many methods of chest X-ray analysis have been developed for this purpose. In this article, the performance of a deep learning algorithm was evaluated, varying three of its parameters: dropout rate, number of neurons in the fully-connected layer (FCL) and pooling layer type, applied to the classification of lung diseases in children. A Convolutional Neural Network (CNN) with MobileNet architecture was applied on 5,241 pediatric chest X-ray images. The best results were for configurations of 32 neurons in the FCL and average pooling for down sampling. Thus, the combination of the variation of the three parameters mentioned with two values in each one, a total of eight CNNs were trained and evaluated. The networks that showed the best results were configured with 0.5 and 0.7 dropout, 32 dense layer neurons and the medium pooling layer.

Keywords: X-ray, Neural Network, MobileNet.

Aplicação da Rede Neural Convolucional MobileNet para a classificação de imagens pediátricas de raio-x de tórax

Resumo: Doenças pulmonares são um problema sério na vida de muitas pessoas e seu diagnóstico correto é extremamente importante. Por esse motivo, muitos métodos de análise de raios-X de tórax foram desenvolvidos. Neste artigo, foi avaliado o desempenho de um algoritmo de aprendizado profundo, variando três de seus parâmetros: taxa de abandono, número de neurônios na camada totalmente conectada (FCL) e tipo de camada de *pooling*, aplicada à classificação de doenças pulmonares em crianças. Uma Rede Neural Convolucional (CNN) com arquitetura *MobileNet* foi aplicada em 5.241 imagens de raios-X de tórax pediátricos. Os melhores resultados foram para configurações de 32 neurônios no FCL e *pooling* médio para *down sampling*. Desta forma, a combinação da variação dos três parâmetros citados com dois valores em cada um, foram treinadas e avaliadas um total de oito CNNs. As redes que demonstraram os melhores resultados foram

configuradas com 0,5 e 0,7 de taxa de abandono, 32 neurônios na camada densa e a camada de *pooling* médio.

Palavras-chave: Raios-X, Rede Neural, MobileNet.

1. Introduction

Chest radiography is one of the most efficient and simple techniques for examining medical images. It allows the production of images of the lungs, heart, airways and other areas. Its interpretation can allow the diagnosis of several types of diseases, including pneumonia, interstitial lung diseases, pneumothorax, nodule in the lung, bone fracture, among others.

However, identifying anomalies on chest radiographs is not always a trivial task, even for the most experienced radiologists. Thus, the development of a diagnostic aid system for radiologists is of great importance. Recently, deep neural networks have been widely studied and applied to medical diagnosis problems (YAMASHITA *et al.*, 2018). Deep Learning refers to machine learning models that have their deepest structure, giving it a better ability to obtain higher levels of abstraction from the input data. Deep neural networks, specifically Convolutional Neural Networks (CNN), have gained a lot of attention in the medical field due to the great effectiveness in image classification problems (MINNEMA *et al.*, 2018).

In this context, image classifiers based on deep learning have been achieving excellent predictive performance, in some cases showing performance superior to that of human specialists in such activities, such as the results obtained in the works of BUETTI-DINH *et al.* (2019), AVENDI *et al.* (2016) and KRIZHEVSKY *et al.* (2012).

This article presents the application of a recent CNN architecture, known as MobileNet, for the classification of chest X-ray images with fifteen different classes: atelectasis, consolidation, infiltration, pneumothorax, edema, emphysema, fibrosis, effusion, pneumonia, thickening pleural, cardiomegaly, nodule, hernia, lung mass and “no findings”, for images without anomalies. Figure 1 shows some images of the most common diseases in the database used. Predictive performance is evaluated comparatively for eight different MobileNet architectural configurations.

Figure 1 - Examples of diseases on chest x-ray

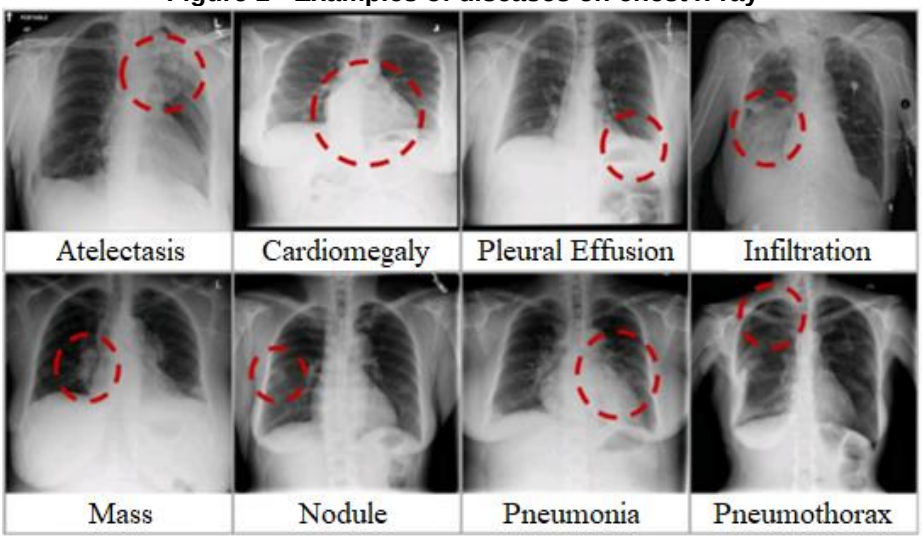

Font: Adapted from Wang *et al.* (2019)

2. Convolutional Neural Networks (CNN)

Neural networks are computational models of machine learning inspired by biological neural networks. These networks are widely used in pattern recognition tasks, such as image recognition, speech recognition, object detection, among others (HAFEMANN, 2014). Since

1990s have been development of Machine Learning algorithms a specialized area of research in Artificial Intelligence (AI) and based of human sensory response (KHAN *et al.*, 2020).

The most basic model of neural networks, composed of a single neuron, is called Perceptron (GAD, 2018). This model is able to recognize patterns, but in a limited way, as it groups only the data that are linearly separable. An alternative to deal with non-linear problems, as is the case with most problems in the real world, is the Multilayer Perceptron (MLP) neural network. MLP is a generalization of Perceptron, so that the sets of neurons are arranged in multiple layers.

The difficulty of traditional algorithms in dealing with problems such as computer vision and speech recognition motivated the development of Deep Learning (DL) algorithms. Deep Learning algorithms are about MLP neural network architectures with more than two hidden layers and techniques that train these models efficiently. In addition, DL is a powerful tool to make a classifier, in this way, the machine will recived the data and find what features use in order to get it done this (GAD, 2018). The increase in the number of layers of a neural network results in a considerable increase in the number of parameters that must be adjusted in the learning algorithm.

There are two crucial factors for deep learning to be able to perform satisfactorily: computational power and data volume. Therefore, deep learning only became viable due to the lower cost of sensors and other equipment capable of generating huge volumes of data for the training of a network and the increased processing capacity of machines with Graphic Processing Unit (GPU). Moreover, the connections between neurons has two characteristics: the weight and the bias, that impact on time to train such networks, and in some cases, it is impossible to train neural networks on machines that have limited GPU and memory capabilities (GAD, 2018).

The Convolutional Neural Networks (CNN) are MLP architectures that mimics the human processing of Visual Cortex, and are one of the best features to classificate image content. Design of CNN was inspired by Hubel and Wisel's work (KHAN *et al.*, 2020). Furthermore, these applications are widely used in deep learning in tasks such as image classification, object tracking, text detection and recognition, action recognition, scenario classification, among others (RAMACHANDRAN, 2015). CNN have shown a high capacity to extract features with medium and high levels of abstraction from image data. Like other MLPs, these neural networks consist of an input layer, multiple hidden layers and an output layer. The hidden layers are composed of the convolution, pooling and fully-connected layers (FCL).

Figure 2 shows a CNN that presents the diagnosis from chest X-ray images. In architecture, convolutional layers are responsible for extracting features. Pooling layers reduce the dimensionality of the network. The FCL are at the end of the neural network to determine its output, by connecting it with all the outputs of the previous layer and making use of an activation function.

Figure 2 - CNN architecture

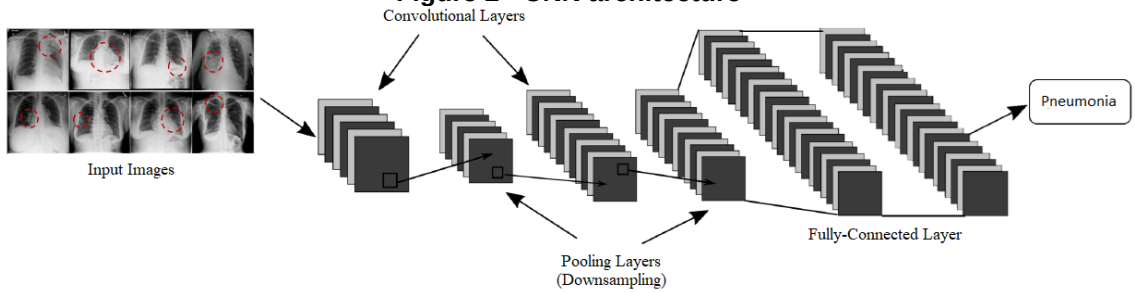

Font: authors (2020)

In image classification tasks, entries are treated as matrices. The length and width of the matrix varies according to the dimensions of the image, while the depth is determined by the number of color channels that form it, with gray scale and Red-Green-Blue (RGB) being the most frequently used.

The convolutional layer is one of the main units of a CNN, and it is where most of the calculations are involved. This layer is composed of non-linear filters that sequentially go through the input data and then produce matrices known as features maps. During the training process, these filters are automatically adjusted so that they are activated in the presence of relevant features, such as the orientation of the edges, lines or color spot. Filters are applied to each convolutional layer and the feature maps are then stacked, forming a matrix with one dimension more than the original dimension of the images.

A limitation of the outputs of the convolutional layers is that they record the exact position of the features of the input images. In other words, this means that a small change in the position of the input image feature will result in a different activation map (RANZATO *et al.*, 2007). This change in input may come from cropping, shifting or rotating the image.

A commonly used approach to deal with this problem is the addition of a pooling (down sampling) layer. In this process, a reduced version of the input image is created, discarding some details, but maintaining structural elements important for classification. There are several ways to perform the down sampling, among them are Max Pooling and Average Pooling. Max Pooling, most often used in image processing, consists of reducing the size of the input layer by taking the maximum values for each region. Thus, this procedure eliminates negligible values, creating invariance to small local distortions. In Max Pooling, a filter compares the numbers contained in the input and chooses the one with the highest value, which is added to the output matrix. After this operation, the filter “slides” over the image according to the step size (stride). Average Pooling, in turn, instead of choosing the highest value, averages the values contained in the layer.

Another important concept in the context of CNN is the dropout. Dropout is a regularization technique that consists of randomly “shutting down” at each training iteration a percentage of the neurons in a layer, re-adding them in the next iteration. This process allows the network to learn more. robust attributes, since a neuron cannot depend on the specific presence of other neurons.

The FCL, in turn, are dense layers in which all of their neurons are connected to all of the neurons in the anterior layer. In the FCL, the features extracted in the convolutional and pooling layers are classified and at the end of it, an activation function, usually a Softmax, is applied to predict the class of the input image.

Activation functions are non-linear functions connected to the end of each neuron. Also inspired by the biological process, these functions determine the output signal based on the input signal and the activation threshold. Other examples of common activation functions, depending on the application, include: sigmoid, hyperbolic tangent and ReLu.

2.1 Convolutional Neural Networks to classification images of X-ray

Sahlol *et al.*, (2020), propouse a method for classification of chest X-ray images using MobileNet, a CNN model, which was previously trained on the ImageNet dataset. The authors, applies the method to diagnostics tuberculosis, which is an infectious disease that attacks the lungs. It selected 25 best features for Shenzen, and 19 best features for Dataset 2. The paper conclude that classification accuracy was 90.2% for Shenzen and 94.1% for Dataset 2.

On the other hand, the paper of Gündel *et al.*, (2018), proposed a location aware Dense Network to detect pathologies in chest X-ray images. Method was applied in a community

that containing 86,876 patients and 297,541 chest X-ray images. Additionally, to multi-label setup, they used a variant of DenseNet with 121 layers, and each output was normalized with a sigmoid function to [0,1]. Gündel *et al.*, (2018) conclude that they research has potential to support throughput reading of the radiologist, to gain more confidence by asking an artificial intelligence system a second opinion.

Apostolopoulos and Mpesiana (2020), applied CNN architectures VGG19 and MobileNetV2 to classificate x-ray images from 3 types of patients: common bacterial pneumonia, COVID-19 and normal incidents. The researchers used two datasets, and concluded that classification accuracy on Dataset 1 of MobileNet V2 was higher effective than VGG19 for specific classification task, and for Dataset 2 the MobileNet V2, distinguished the COVID-19 cases from other cases of dataset.

Finally, the work of Togaçar, Egen and Cömert (2020) used Deep Learning models MobileNet V2 and SqueezeNet to classify x-ray images and detect COVID-19 disease. The authors, trained dataset with these two deep learning models and the result obtained were processed using the Social Mimic optimization method, they conclude that work obtained a classificate rate of the proposed approach was 99.27%.

2.2 MobileNet

In 2017, Howard *et al.* (2017) proposed a new class of CNN called MobileNet. Designed to be a small network, it allows faster and easier integration into applications for mobile devices. Moreover, Togaçar, Egen and Cömert (2020), presents MobileNet as a deep learning model to be used in low hardware cost devices. Due to its Depthwise Separable Convolution strategy, MobileNet has reduced its computational complexity. Figure 3 shows the architecture of this CNN.

Figure 3 - MobileNet architecture

Type / Stride	Filter Shape	Input Size
Conv / s2	$3 \times 3 \times 3 \times 32$	$224 \times 224 \times 3$
Conv dw / s1	$3 \times 3 \times 32$ dw	$112 \times 112 \times 32$
Conv / s1	$1 \times 1 \times 32 \times 64$	$112 \times 112 \times 32$
Conv dw / s2	$3 \times 3 \times 64$ dw	$112 \times 112 \times 64$
Conv / s1	$1 \times 1 \times 64 \times 128$	$56 \times 56 \times 64$
Conv dw / s1	$3 \times 3 \times 128$ dw	$56 \times 56 \times 128$
Conv / s1	$1 \times 1 \times 128 \times 128$	$56 \times 56 \times 128$
Conv dw / s2	$3 \times 3 \times 128$ dw	$56 \times 56 \times 128$
Conv / s1	$1 \times 1 \times 128 \times 256$	$28 \times 28 \times 128$
Conv dw / s1	$3 \times 3 \times 256$ dw	$28 \times 28 \times 256$
Conv / s1	$1 \times 1 \times 256 \times 256$	$28 \times 28 \times 256$
Conv dw / s2	$3 \times 3 \times 256$ dw	$28 \times 28 \times 256$
Conv / s1	$1 \times 1 \times 256 \times 512$	$14 \times 14 \times 256$
$5\times$ Conv dw / s1	$3 \times 3 \times 512$ dw	$14 \times 14 \times 512$
$5\times$ Conv / s1	$1 \times 1 \times 512 \times 512$	$14 \times 14 \times 512$
Conv dw / s2	$3 \times 3 \times 512$ dw	$14 \times 14 \times 512$
Conv / s1	$1 \times 1 \times 512 \times 1024$	$7 \times 7 \times 512$
Conv dw / s2	$3 \times 3 \times 1024$ dw	$7 \times 7 \times 1024$
Conv / s1	$1 \times 1 \times 1024 \times 1024$	$7 \times 7 \times 1024$
Avg Pool / s1	Pool 7×7	$7 \times 7 \times 1024$
FC / s1	1024×1000	$1 \times 1 \times 1024$
Softmax / s1	Classifier	$1 \times 1 \times 1000$

Font: Howard *et al.*, 2017

The MobileNet architecture available in the Keras library documentation presents the pre-trained network in the ImageNet database, which is an image bank that contains more than 14 million images divided into more than 20,000 categories. Details of MobileNet can be obtained at: https://keras.io/applications/#mobilenet.

To realize the experiments of this work, was applied the code developmented by Kevin Mader (2017), which is disponibilied on the Kaggle platform, the author used the code to classify dataset of integral form (with adults and pediatrics datas).

3. Materials and methods

In this article, for training and validation of MobileNet models, a subset consisting of pediatric images from the benchmark data set known as “NIH Chest X-rays” was used, available at: https://www.kaggle.com/nih-chest-xrays/data. Originally, this set contains 112,120 frontal chest X-ray images of more than 30,000 patients (including adults and pediatricians), and is available from the National Institutes of Health of United States of America (NIH). To select only pediatric patients, the focus of this article, we selected only images whose values for the feature “PatientAge” were less than eighteen years old. Figure 4 shows the distribution of the frequency of ages in the subset of pediatric images.

Figure 4 - Frequency distribution of pacients’ ages

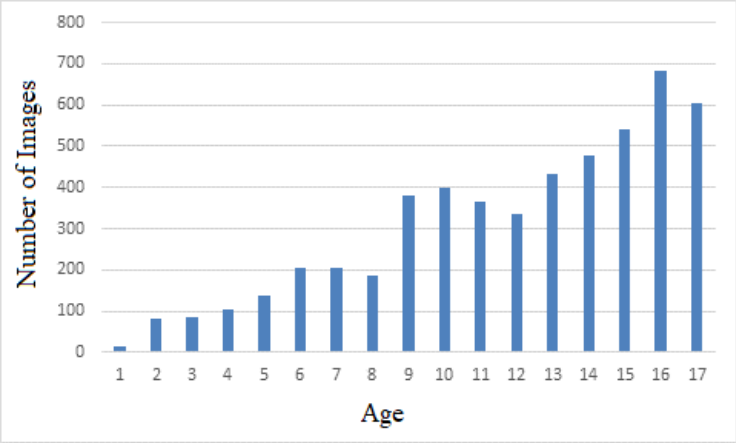

Font: authors (2020)

Considering this selection, the data set used was composed of 5,241 pediatric images labeled with one or more of the 13 pathologies and, if the radiography had not presented any anomaly, the image was labeled with “no findings” (WANG *et al.*, 2019). Figure 5 shows the distribution of the data set according to the pathologies found in each image.

Figure 5 - Distribution of the classes of the pediatric data set

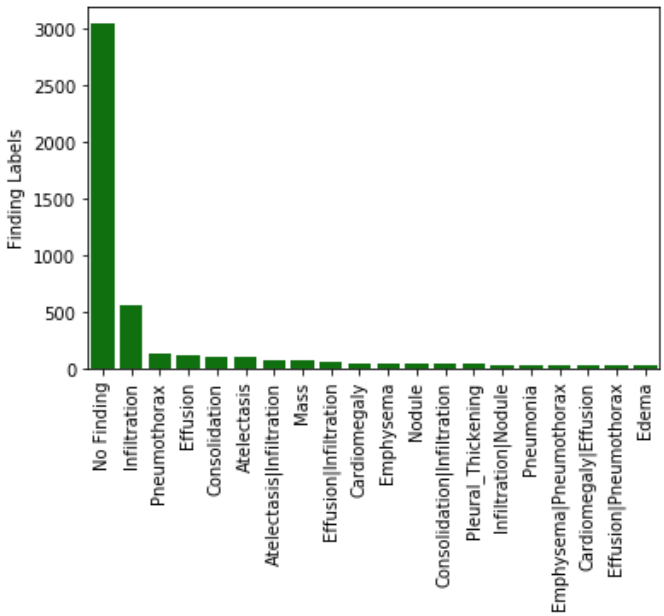

Font: authors (2020)

A total of eight experiments were performed (each of which is a different MobileNet configuration) with 50 iterations each. The performance criterion for comparatively evaluating the eight configurations was the Area Under Curve (AUC) weighted by the number of occurrences of each disease. The settings for each experiment are shown in Table 1.

Table 1 - Configurations of the experiments

Experiment	Downsampling	Number of neurons in the FCL	Dropout rate
A	Average Pooling	32	0,5
B	Average Pooling	32	0,7
C	Average Pooling	64	0,5
D	Average Pooling	64	0,7
E	Max Pooling	32	0,5
F	Max Pooling	32	0,7
G	Max Pooling	64	0,5
H	Max Pooling	64	0,7

Font: authors (2020)

The algorithms were implemented in the development environment Spyder (version 3.3.6) in Python language (version 3.7.3). The choice of this language is due to its widespread use in academia, its syntax is relatively simple. In addition, its flexibility allows interaction with other software. All executions of the algorithms were performed using a Samsung Odyssey notebook with an Intel Core i7 - 7th generation 2.8GHz processor, and 8 GB of RAM. The computer has an NVIDIA GeForce GTX 1050 video card and Windows 10 Pro 64-bit operating system.

4. Results analysis

Initially, for each experiment, the images were classified, with one disease attributed to each image. No cases of hernia were found in the set of pediatric images, so this class was removed before the classification algorithms were run. The most common predicted class was “No Findings”, which actually does not represent any disease. Thus, a treatment was applied to remove all instances whose classes were “No Findings” as a way of trying to balance the prevalence of classes to a certain extent. In order to generate new copies of training data to increase the capability of generalizability of the model, a data augmentation procedure was also applied as well. The percentage of images classified as being for each disease for each experiment is shown in Table 2. The column called “Actual” shows the actual prevalence of each disease in the data set and the remaining columns are the percentages of instances predicted to belong to each disease.

Table 2 - Classification results

	Actual	Predicted (%)							
	(%)	A	B	C	D	E	F	G	H
Atelectasis	7.52	3.40	7.63	11.65	9.11	6.09	7.97	5.76	1.97
Cardiomegaly	3.47	2.79	10.96	1.26	9.15	0.07	2.42	4.09	5.22
Consolidation	5.51	4.94	5.51	5.91	4.65	3.09	3.56	1.86	1.11
Edema	2.98	0.67	4.00	0.53	3.65	2.69	0.45	1.39	0.52
Effusion	11.18	6.90	14.71	8.59	12.27	1.51	5.22	5.85	1.08
Emphysema	1.11	0.43	0.49	1.37	2.80	0.71	0.17	0.98	0.77
Fibrosis	0.34	0.66	0.37	0.21	0.04	0.11	0.08	0.08	1.71
Infiltration	24.04	11.37	17.52	25.91	14.25	8.98	11.62	21.15	11.85
Mass	3.47	3.15	7.50	4.21	2.58	0.25	4.12	1.01	2.02
Nodule	4.39	0.46	4.01	1.58	2.46	1.83	0.53	1.13	5.80
Pleural Thickening	2.57	0.34	0.72	1.06	0.62	0.13	0.63	0.81	4.58
Pneumonia	2.17	1.35	14.05	2.97	1.83	1.82	0.21	1.60	5.32
Pneumothorax	4.73	3.26	4.04	6.74	2.62	1.98	3.26	0.59	3.00

Font: authors (2020)

After that, the AUC values for each disease were obtained. The results indicated that experiments A and B obtained better average performances among all experiments, with AUC value of 0.59, while experiment D was the one that presented the worst performance, with AUC of 0.55. These AUC values are presented in Table 3. As explained at the beginning of this section, the class “No Findings”, was suppressed before run the classification.

Table 3 - AUC values

	A	B	C	D	E	F	G	H
Atelectasis	0.55	0.63	0.59	0.57	0.55	0.55	0.53	0.56
Cardiomegaly	0.64	0.65	0.55	0.59	0.60	0.58	0.63	0.61
Consolidation	0.59	0.56	0.56	0.55	0.59	0.60	0.59	0.61
Edema	0.67	0.63	0.57	0.63	0.64	0.59	0.64	0.65
Effusion	0.62	0.63	0.62	0.64	0.63	0.67	0.61	0.62
Emphysema	0.62	0.51	0.62	0.48	0.56	0.51	0.69	0.40
Fibrosis	0.52	0.56	0.48	0.37	0.57	0.58	0.52	0.48
Infiltration	0.58	0.57	0.56	0.57	0.54	0.55	0.59	0.55
Mass	0.58	0.60	0.52	0.54	0.63	0.53	0.52	0.57
Nodule	0.59	0.55	0.55	0.55	0.51	0.52	0.48	0.57
Pleural Thickening	0.61	0.67	0.56	0.62	0.60	0.57	0.53	0.62
Pneumonia	0.54	0.58	0.54	0.49	0.51	0.53	0.45	0.56
Pneumothorax	0.57	0.59	0.51	0.58	0.51	0.55	0.60	0.56
Average	**0.59**	**0.59**	**0.56**	**0.55**	**0.57**	**0.56**	**0.57**	**0.57**

Font: authors (2020)

Using the values in Table 2 as a basis, the weighting mentioned above was applied, multiplying the AUC values for each class by the corresponding disease incidence. This procedure was carried out with the objective of better comparison between the curves of the different diseases, as there is a great imbalance between the quantity of each one. Among the eight experiments carried out, considering such weightings, the CNN that presented the

best performances were those with 32 neurons in the FCL and with Average Pooling for downsampling, that is the experiments A and B again. Their performances were 0.4350 and 0.4385, respectively. The experiment D set up with Average Pooling, 64 neurons in the FCL and dropout rate of 07, presented the worst results as well, with 0.3742. The results are shown in Table 4.

Table 4 - Weighted AUC

	A	B	C	D	E	F	G	H
Atelectasis	0.0414	0.0474	0.0444	0.0429	0.0414	0.0414	0.0399	0.0421
Cardiomegaly	0.0222	0.0226	0.0191	0.0540	0.0208	0.0201	0.0219	0.0212
Consolidation	0.0331	0.0314	0.0314	0.0256	0.0331	0.0337	0.0331	0.0342
Edema	0.0200	0.0188	0.0170	0.0230	0.0191	0.0176	0.0191	0.0194
Effusion	0.0693	0.0704	0.0693	0.0785	0.0704	0.0749	0.0682	0.0693
Emphysema	0.0069	0.0057	0.0069	0.0134	0.0062	0.0057	0.0077	0.0044
Fibrosis	0.0018	0.0019	0.0016	0.0001	0.0019	0.0020	0.0028	0.0016
Infiltration	0.1394	0.1370	0.1346	0.0812	0.1298	0.1322	0.1418	0.1322
Mass	0.0201	0.0208	0.0180	0.0139	0.0219	0.0184	0.0180	0.0198
Nodule	0.0259	0.0241	0.0241	0.0135	0.0224	0.0228	0.0211	0.0250
Pleural Thickening	0.0163	0.0179	0.0150	0.0038	0.0160	0.0152	0.0142	0.0166
Pneumonia	0.0117	0.0126	0.0117	0.0090	0.0111	0.0115	0.0098	0.0122
Pneumothorax	0.0270	0.0279	0.0241	0.0152	0.0241	0.0260	0.0284	0.0265
Total	**0.4350**	**0.4385**	**0.4173**	**0.3742**	**0.4182**	**0.4214**	**0.4248**	**0.4245**

Font: authors (2020)

5. Final considerations

This article proposed to compare MobileNet with different types of layer pooling, dropout rate and number of neurons in the FCL. MobileNet, known for its simplicity when compared to others, stands out for its effectiveness in computer vision tasks and speed in training. Using CNN pre-trained in the ImageNet database, MobileNet has been trained, validated and tested with NIH Chest X-ray pediatric data using each of the eight proposed configurations. All results show that experiments A and B performed better with the pediatric images from the NIH Chest X-ray dataset and experiment D had the worst performance in the classification of images.

Although, compering the results of AUC presented in study, it is necessary improve the architecture configuration, because compered the best results obtained are bottom of others in different architecture, like the work of Bar Y. *et al.* (2015) which in some CNNs of x-ray images performed with results between 0,72 and 0,92.

As the present investigation is still ongoing and considering what was intended with this stage of the research, the results were considered satisfactory. As future research it is suggested to compare the performance of MobileNet with other CNN architectures in the literature, from the classic LeNet-5, AlexNet and VGG16 and the modern Inception, ResNet, ResNeXt and DenseNet. Another future perspective is the application of combinatorial optimization for hyperparameters fine tuning.

References

AVENDI, M. R., KHERADVAR, A., JAFARKHANI, H. A combined deep-learning and deformable-model approach to fully automatic segmentation of the left ventricle in cardiac MRI. **Medical Image Analysis,** v. 30, n. 7, p. 108-119, 2016. Available in: https://doi.org/10.1016/j.media.2016.01.005. Access: 01 Sep. 2020.

APOSTOLOPOULOS, I. D.; MPESIANA, T. A. Covid-19: automatic detection from X-ray images utilizing transfer learning with convolutional neural networks. **Physical and Engineering Sciences in Medicine,** v. 43, p. 635–640, 2020. Available in: https://doi.org/10.1007/s13246-020-00865-4. Access: 01 Sep. 2020.

BAR, Y. *et al*. Deep learning with non-medical training used for chest pathology identification. *In:* **SPIE medical imaging**, Orlando, v. 9414, p. 7, 2015.

BUETTI-DINHA, A. *et al*. Deep neural networks outperform human expert's capacity in characterizing bioleaching bacterial biofilm composition. **Biotechnology Reports**, v. 22, p. 108–119. 2019. Available in: https://doi.org/10.1016/j.btre.2019.e00321. Access: 22 Ago. 2020.

GAD, A. F. **Practical computer vision applications using deep learning with CNNs:** With Detailed Examples in Python Using TensorFlow and Kivy. New York: Apress, 2018. E-book. ISBN: 978-1-4842-4167-7Available in: https://doi.org/10.1007/978-1-4842-4167-7. Access: 29 ago. 2020.

GUENDEL, S. *et al*. Learning to recognize abnormalities in chest x-rays with location-aware dense networks. *In*: Iberoamerican Congress on Pattern Recognition, 2018. p. 757-765, nov. 2018. Available in: https://arxiv.org/pdf/1803.04565.pdf. Access: 30 ago. 2020.

HAFEMANN, L. G. **An analysis of deep neural networks for texture classification.** Master's degree Dissertation. M Sc. Program in Informatics, University Federal of Paraná, Curitiba, 2014.

HOWARD, A. G. *et al*. MobileNets: efficient convolutional neural networks for mobile vision applications. 2017. Available in: arXiv:1704.04861. Access: 12 Sep. 2020.

KHAN, A. *et al*. A survey of the recent architectures of deep convolutional neural networks. **Artificial Intelligence Review**. 2020. Available in: https://doi.org/10.1007/s10462-020-09825-6

KRIZHEVSKY, A.; SUTSKEVER, I.; HINTON, G. E. ImageNet classification with deep convolutional neural networks. **Advances in neural information processing systems**, v. 5, n. 7, p. 1097-1105, 2012.

MINNEMA, J. *et al*. CT image segmentation of bone for medical additive manufacturing using a convolutional neural network. **Computers in Biology and Medicine**, v. 103. p. 130–139. 2018. Available in: https://doi.org/10.1016/j.compbiomed.2018.10.012. Access: 22 Ago. 2020.

RAMACHANDRAN, R. *et al*. Deep learning an overview. **IJAER**. v. 10, p. 25433-25448. 2015.

RANZATO, M. A. *et al*. Unsupervised learning of invariant feature hierarchies with applications to object recognition. **IEEE Conference on Computer Vision and Pattern Recognition**. p 1-8. 2017.

SAHLOL, A.T. *et al*. A novel method for detection of tuberculosis in chest radiographs using artificial ecosystem-based optimization of deep neural network features. **Symmetry**, v. 12, n. 1146. 2020. Available in: https://doi.org/10.3390/sym12071146. Access: 12 Sep. 2020.

TOGAÇAR, M.; ERGEN, B; CÖMERT, Z. COVID-19 detection using deep learning models to exploit Social Mimic Optimization and structured chest x-ray images using fuzzy color and stacking approaches**. Computers in Biology and Medicine**, v. 121, n. 103805, 2020. Available in: https://doi.org/10.1016/j.compbiomed.2020.103805. Access: 01 Sep. 2020.

WANG, X. *et al*. Chest x-ray: hospital-scale chest x-ray database and benchmarks on weakly supervised classification and localization of common thorax diseases. **Deep Learning and Convolutional Neural Networks for Medical Imaging and Clinical Informatics**, p. 369-392. 2019.

YAMASHITA, R. *et al*. Convolutional neural networks: an overview and application in radiology. **Insights into Imaging**, v. 9, p. 611–629. 2018.